Proceedings of the ASME 2020 39th International Conference on Ocean, Offshore and Arctic Engineering
OMAE2020
August 3-7, 2020, Virtual, Online

OMAE2020-18355

NUMERICAL SIMULATION OF HYDRODYNAMICS AROUND NET MESHES USING REEF3D

Gang Wang[1]
Department of Civil and Environmental Engineering,
Norwegian University of Science and Technology
7491 Trondheim, Norway
College of Fisheries, Ocean University of China
266003 Qingdao, China

Tobias Martin
Department of Civil and Environmental Engineering,
Norwegian University of Science and Technology
7491 Trondheim, Norway

Liuyi Huang
College of Fisheries, Ocean University of China
266003 Qingdao, China

Hans Bihs
Department of Civil and Environmental Engineering,
Norwegian University of Science and Technology
7491 Trondheim, Norway

ABSTRACT

Hydrodynamics and turbulence around net meshes have drawn more and more attention because it is closely related to forces on the structures and safety issues of offshore fish farms. In terms of numerical modeling of forces on nets, Morison or screen force model is ordinarily adopted to account for its hydrodynamics. However, these methodologies mainly rely on empirical experimental or cylindrical hydrodynamic coefficients, neglecting flow interactions between adjacent cruciforms or net bars. In this study, REEF3D open-source hydrodynamic toolbox is adopted to analyze flow around net meshes explicitly and investigate the hydrodynamics related to forces on the structure. The simulation accuracy is in good agreement with flume experiments and previous research. Flow velocity and vorticity around net bars and knots are investigated. The results demonstrate that 2×2 or 3×3 mesh cases are more reliable when studying turbulence around net meshes, flow interactions around adjacent net bars, knots should be taken into consideration. Two patterns to control S_n, one is to change the diameter of net bars and the other is to control length, have different effects on the flow around meshes. This paper presents a first step in the aim to derive a new empirical formula for C_d depending on S_n, and Re, which are more related to the physics in offshore conditions.

Keywords: Fishing nets; Hydrodynamics; CFD; Drag forces

1 INTRODUCTION

Nowadays, due to the pollution and the increase of aquaculture in coastal areas, the fish farming industry tends to move to offshore area and fish cage system would become much larger and more complicated compared with the traditional fish cage. Meanwhile, since the sea environment loadings in deep water is more severe compared to near-shore area, fish farms would undergo extreme dynamic response or deformation of nets, leading to fatigue or unpredictable damage of components of fish cages. The failure of offshore cage systems mainly comes from operational mistakes, breakage of mooring lines and the collision between chains and nets [1]. Nets of fish farms endure extreme wave-current loadings and have the risk of collision with fish and other animals, leading to the damage of net meshes [2]. The hydrodynamics around each net mesh used in offshore fish farms is still not investigated with respect to turbulence effects. Therefore, it is crucial to study the flow around net meshes adopted in offshore fish farms.

Unlike typical marine structures of offshore engineering, diameters and lengths of net meshes in full scale are small, while other components of fish farms are of the size of incident waves. It would cause great difficulties in carrying out flume experiments if the details of the flow around the net meshes and inside cages are of interest. Besides, flow conditions inside the fish cage using Computational Fluid Dynamics (CFD) considering deformations of nets is still ongoing research [3]. It is feasible to study the turbulence and hydrodynamics of net meshes using CFD, providing a more intuitive understanding

[1] Contact author: gang.wang@ntnu.no

about the flow around meshes. Numerous researchers have estimated the hydrodynamics around net panels and proposed different semi-empirical formulas based on experiments, but no standard coefficients were adopted considering various structural factors, and the detailed turbulence around the net meshes remained unclear. Normal and tangential drag coefficient (C_d) of each mesh bar based on Reynolds number (Re) were studied in [4], but other structural factors or interactions among net bars were not included. In [5], a relation between the normal C_d and solidity ratio (S_n) applied to square net meshes of knotless and nets with knots were derived using experiments. As presented in [6], C_d and the lift coefficient of net panels related to S_n and the Angle of Attack (AOA) were analyzed based on experiments, especially the irrelevance between C_d and AOA when the panel was parallel to the incoming flow, that is, AOA=0° was emphasized. Considering the hydrodynamics around net meshes more comprehensively, it is insufficient to use S_n as the only parameter, and parameters related to turbulence around meshes should also be investigated. In [7], normal and tangential C_d were deduced as the function of velocity and S_n based on the experiments of Nylon plane nets with diamond meshes. The analytical C_d of cylinders proposed by [8] was revised in [9], taking Re and S_n into consideration at the same time. As shown in [10], a hydrodynamic flume test of Nylon fishing nets was carried out. The results for Re ranging from 430 to 5742 and AOA ranging from 10° to 90° showed dependencies of C_d on these two factors. However, the impact of Re on the lift force could be ignored, so lift coefficient was only dependent on AOA. Except for the Morison model, the screen net model, which calculates the deformation of nets based on hydrodynamics of net panel, was developed in [11]. In [12], flume experiments were adopted to analyze the hydrodynamics of a cruciform structure representing a single net mesh. Moreover, a semi-empirical formula was derived experimentally by studying hydrodynamics of plane nets, combining S_n with AOA and Re [13~14]. However, because the research mainly studied meshes of purse seine with small S_n, hydrodynamics of nets with a wide range of S_n were not discussed. In terms of turbulence around nets, the flow around nets was modelled numerically using porous media in [15~18, 36]. Here, flow fields downstream of nets and the velocity reduction effects were simulated, but details regarding turbulence around the net meshes were lacking. Afterwards, a high-resolution CFD simulation of the flow around net meshes was investigated in [19], velocity profiles around meshes were extracted and the influence of the AOA and mesh orientation on the turbulence were analyzed specifically.

It is therefore of interest to carry out high-resolution numerical simulations of the turbulence and hydrodynamics around net meshes in order to improve existing numerical models for fluid-net interaction. 1×1, 2×2 and 3×3 meshes are considered and a comparison of the turbulent interaction of fluid and different net meshes is presented. The structural response of the net is neglected because of the small geometrical scale. As the main parameters of the meshes, S_n and Re are chosen. The simulations are performed using the open-source CFD code REEF3D [20]. The code has been verified and validated for a wide range of marine applications, such as breaking wave forces [21, 33~35] and fluid-structure interaction of floating structures and nets [22, 36~37].

In the following, details about the chosen geometry for the net meshes and the numerical methods were presented. Then, the results of the simulations are shown with respect to turbulence and the hydrodynamics around the net meshes with varying S_n and Re. A semi-empirical formula is proposed based on the numerical simulations.

2 Material and methods

2.1 Net meshes

The net meshes analyzed in this research is the prototype used in the inner nets of Deep Blue I, the largest offshore fish farm in China (Fig. 1). In general, inner nets are exposed to several kinds of loading, including fluid loading and interactions with fish. The prototype has the square twisted knotless meshes with a constant solidity ratio of 0.28, of which diameter and length of the mesh bar is 3mm and 2cm, respectively (Fig. 1). The material of nets is Ultra High Molecular Weight Polyethylene Fiber (UHMWPE), which is widely used in the fields of aviation and ocean industry.

FIGURE 1: Deep Blue I and its prototype mesh

2.2 Numerical modeling

The incompressible fluid flow is described by the three-dimensional Unsteady Reynolds-Averaged Navier-Stokes equations (URANS), which are solved together with the continuity equation for prescribing momentum and mass conservation (Eq. 1)

$$\frac{\partial u_i}{\partial x_i} = 0 \tag{1}$$

$$\frac{\partial u_i}{\partial t} + u_j \frac{\partial u_i}{\partial x_j} = -\frac{1}{\rho}\frac{\partial p}{\partial x_i} + \frac{\partial}{\partial x_j}\left[(\nu + \nu_t)\left(\frac{\partial u_i}{\partial x_j} + \frac{\partial u_j}{\partial x_i}\right)\right] + g_i$$

where u is the velocity averaged over time t, ρ is the fluid density, p is the pressure, v is the kinematic viscosity, v_t is the eddy viscosity and g the acceleration due to gravity. The eddy viscosity v_t in the URANS equations is modelled using the two-equation k-ω model [23], and it is combined with level set method in REEF3D.

The convective and diffusion terms of the URANS equations are discretized with the third-order WENO scheme [20] in the conservative finite-difference framework. For the time treatment of the momentum equations, a third-order accurate TVD Runge-Kutta scheme was employed. Diffusion terms of URANS equations are treated implicitly to ensure the stability of the calculations.

2.3 Boundary condition

A 3D Cartesian right-handed coordinate system is established in the numerical simulation, in which x is positive along the flow direction, z is perpendicular to the flow direction on the horizontal plane and y is perpendicular to the plane formed by x and z. The non-dimensional computational domain is approximately 214d in length, 143d in width and 143d in height, remained the same as [19]. Here, d is the diameter of the cylinder. At the inlet, a uniform velocity is imposed, and zero gradient pressure outflow condition is used at the outlet. The surrounding boundaries in the domain are treated with symmetry conditions, which means the normal components of the velocity are set to zero and the normal gradients of all variables are zero. For initializing the k-ω turbulence model, the turbulent intensity I is given at the inlet boundary based on the equations 2. The surfaces of the net meshes are defined as non-slip wall boundaries, and the near-surface velocity was modelled based on wall functions.

$$D_H = \frac{4A_c}{S_c}; Re_{D_H} = \frac{vD_H}{\nu}; I = 0.16(Re_{D_H})^{-1/8} \tag{2}$$

where A_c and S_c are cross sectional area of computational domain in the x direction and perimeter of this cross section, respectively. D_H is the hydraulic diameter of flume tank and Re represents Reynolds number on the basis of the hydraulic diameter.

2.4 Computational grids: Immersed Boundary method

In REEF3D, a ghost cell immersed boundary method (GCIBM) is used [20]. Thus, the numerical discretization does not need to account for the boundary conditions explicitly. Instead, they are enforced implicitly. In this study, the uniform-sized mesh based on GCIBM was adopted in the whole domain, and the cell number varies between 3.0×10^7 and 2.0×10^8.

2.5 Data statistics and cases set-up

To study hydrodynamics around net meshes, mean values of the drag coefficient C_d are calculated using Eq. 3.

$$C_d = \frac{F_d}{0.5\rho S U^2} \tag{3}$$

where F_d represents the time averaged resistance, S is the projection area of the meshes and U is the incoming velocity.

The Solidity ratio, S_n, describes the ratio of the projected area of the net over the total area, enclosed by the net. For the square mesh in this study, S_n is defined as follows (Eq. 4) [38]

$$S_n = \frac{2*d}{l} - \left(\frac{d}{l}\right)^2 \tag{4}$$

where l and d are the length and diameter of each net bar, respectively. Eq .4 could only be adopted in square meshes of fishing nets.

Typically, vortex motion and its related variation characteristics which could be expressed as the rotation are defined as turbulence structures [24], and the quantitative magnitude of the rotation are visualized by the Q-criterion [25] given in Eq. 5.

$$Q = -\frac{1}{2}(S_{ij}S_{ij} - \Omega_{ij}\Omega_{ij}); S_{ij} = \frac{1}{2}\left(\frac{\partial u_i}{\partial x_j} + \frac{\partial u_j}{\partial x_i}\right) = Sym\left(\frac{\partial u_i}{\partial x_j}\right); \tag{5}$$

$$\Omega_{ij} = \frac{1}{2}\left(\frac{\partial u_i}{\partial x_j} - \frac{\partial u_j}{\partial x_i}\right) = Asym\left(\frac{\partial u_i}{\partial x_j}\right)$$

where S_{ij} is vorticity and Ω_{ij} represents strain rate.

As an important geometrical factor, S_n and Re have the considerable impacts on the hydrodynamics and turbulence around the net mesh. It is closely related with incoming velocity, diameter and length of net bar from a square net mesh. Two methods of changing S_n, diameter and length of each bar, are adopted in this study. All cases are shown in Table 1 as following.

Table 1: Cases set-up

Case	Dimension	How to change S_n and Re	Re	S_n
1	1*1	(Prototype Mesh)	756.30	0.28
2	2*2		756.30	0.28
3	3*3		756.30	0.28
4	2*2	Change diameter of net bar	533.08	0.2
5	2*2		823.56	0.3
6	2*2		1136.49	0.4
7	2*2		1476.77	0.5
8	2*2		1853.17	0.6
9	2*2	Change length of net bar, and change the incoming velocity	756.30	0.2
10	2*2		756.30	0.3
11	2*2		756.30	0.4
12	2*2		756.30	0.5
13	2*2		756.30	0.6
14	2*2		1260.50	0.2
15	2*2		1764.71	0.2
16	2*2		2268.91	0.2
17	2*2		1260.50	0.3
18	2*2		1764.71	0.3
19	2*2		2268.91	0.3
20	2*2		1260.50	0.4
21	2*2		1764.71	0.4
22	2*2		2268.91	0.4
23	2*2		1260.50	0.5
24	2*2		1764.71	0.5
25	2*2		2268.91	0.5
26	2*2		1260.50	0.6

27	2*2		1764.71	0.6
28	2*2		2268.91	0.6
29	2*2		1260.50	0.28
30	2*2		1764.71	0.28
31	2*2		2268.91	0.28

2.6 Validations

To ensure that the turbulence through the net meshes and the hydrodynamics are captured sufficiently, the grid size around the structures has to be sufficiently small. Therefore, a mesh independence test is carried out for the time-averaged drag coefficient (C_d, Eqn. 3). A constant Reynolds number (Re) of 10^5 is used. The computsational domain and the boundary conditions are kept the same as given in [26] to ensure comparability of various methods. The results can be found in Table 2. It is evident that the case with 40 cells (approximately 3.1×10^{-4} m) in the circumference of the cylinder is sufficient to analyze the turbulence around the cylindrical structure. This mesh pattern is adopted in the following studies. In comparison, it would need 60 cells using a conforming mesh strategy and Finite Volume Methods [19].

Table 2: Mesh independence test

Cells in circumference	Cell number	Drag coefficient
16	6.2×10^4	1.286
24	1.4×10^5	1.245
32	2.5×10^5	1.266
40	3.9×10^5	1.138
48	5.6×10^5	1.081
56	7.6×10^5	1.094
64	1.0×10^6	1.014

In addition, the hydrodynamics around a 2D cylinder with a wider range of Re is studied as the following Fig. 2 shows. Within the range of Re from 300 to 10^5, REEF3D predicts C_d with a good agreement with the empirical values and other simulation data, meaning that 40 cells in the circumference of the cylinder seems feasible. Moreover, REEF3D overpredicts the drag forces slightly in the range $10^3 < Re < 2.5 \times 10^3$, which is close to the transition area of laminar to turbulent flow. The deviation is still acceptable because the error was smaller than 8%.

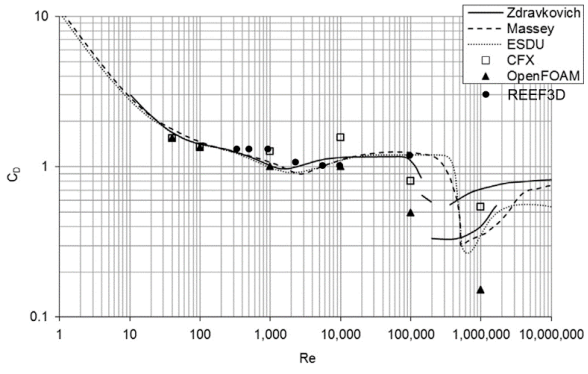

Figure 2: Drag coefficient versus Reynolds number; correlation between experimental and numerical results. Published values for smooth cylinder: Zdravkovich [28], Massey [29], ESDU [30], Norberg [31], Achenbach and Heinecke [32], CFX/OpenFOAM [26].

To test the performance of the flow around a 3D structure, a cruciform case (Fig. 3a), which has been investigated in [19] numerically and in [12] experimentally, is used to validate the accuracy of REEF3D. The results are shown in Fig. 3b. The deviation between the results in [19] and REEF3D are small, which showed the current cell configuration was acceptable to continue the research.

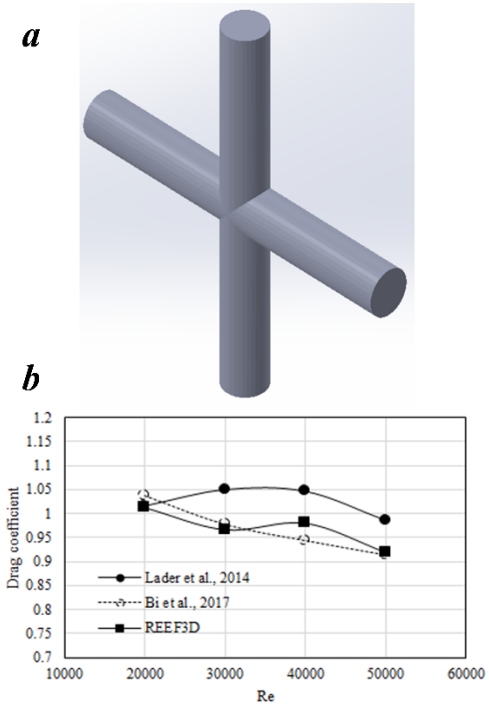

Figure 3: ***a.*** Geometry in cruciform. ***b.*** Drag coefficient vs. Reynolds number for REEF3D and the laboratory experiment on a cruciform element [12].

3 Results and discussion

3.1 Flow around three-sized net meshes

Three cases with different-sized net meshes, which were 1×1 (Case 1), 2×2 (Case 2) and 3×3 (Case 3), are considered to study the flow around meshes and turbulent patterns. The diameter and length of each net bar remained the same as the prototype. Generally, knots and mesh centers of a net panel are the areas with significant turbulence due to local acceleration of the fluid along the twines [27]. Several probe lines in x direction are used to measure the velocity fluctuations at the knots and mesh centers. The incoming velocity is kept at 0.3m/s, with a Re of 700. It is obvious that the velocity drops rapidly at each knot and increases gradually in the downstream area (Fig. 4). It is because the vortex formation appears after flowing through the structures, leading to the negative values of flow velocity. Behind the vortex, the downstream velocity would increase to

incoming velocity based on the conservation laws. The downstream velocity does not exceed the incoming velocity in Case 1 and Case 2, while the velocity at only one knot of Case 3 is slightly larger than the incoming velocity. Case 2 and Case 3 show the similar variation trend while the velocity of Case 1 surges at the front of the knots and fall quickly. The flow interactions around adjacent net bars, knots and effects of mesh interaction account for the difference of variation. In other words, the 2×2 or 3×3 mesh cases were more reliable for studying turbulence patterns than a single mesh.

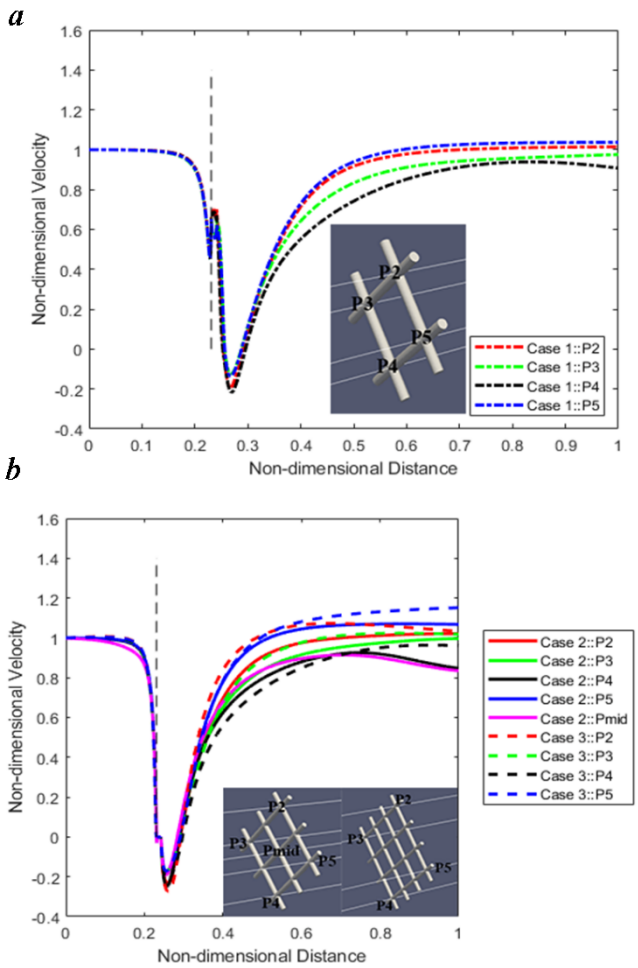

Figure 4: Non-dimensional velocity along the probe lines through the knot positions of three-sized meshes. **Note:** dotted line represents the position of net meshes, same as below. ***a.*** Non-dimensional velocity along the probe lines in Case 1; ***b.*** Non-dimensional velocity along the probe lines in Case 2 and 3.

Fig. 5 shows the velocity profile along the probe lines at the mesh center of each case. It is sufficient to consider the flow of only 6 probe lines in the 9-mesh Case 3 due to its symmetrical characteristics. It is illustrated in Fig.5 that the flow velocity increases sharply and then drops with different slopes at varied downstream distances. The flow in front of the structure is blocked to a little extent by the net itself. Afterwards, a local acceleration of the flow at the mesh center appears because the incoming flow is separated when passing the cylindrical net bars. The velocity reduction is significant as the downstream velocity decreases to around 80% of the incoming velocity. The velocity increases slowly over the distance but is still lower than the incoming velocity. This is due to the declining shielding effect of the net bars. When it comes to comparisons among three-sized meshes, it can be seen that in Case 3 the largest velocity increment occurs, while Case 2 shows the longest distance of velocity reduction in the downstream region. Case 1 shows a significant diversity of the flow patterns compared to the other cases. Here, strong interactions due to nearby meshes are observed.

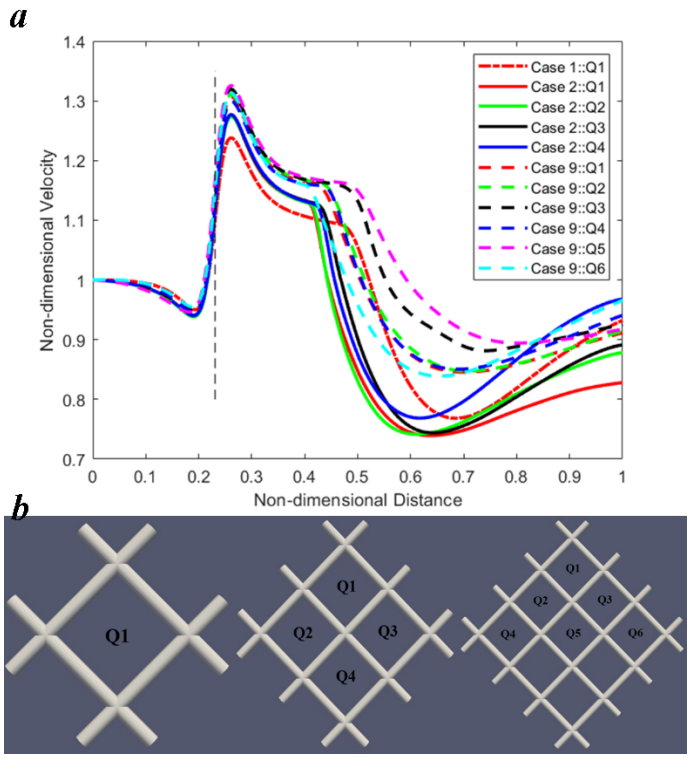

Figure 5: ***a.*** Non-dimensional velocity along the probe lines around mesh center of each case; ***b.*** The positions of each probe lines through incoming stream direction.

In order to study the turbulent structures around the net meshes more specifically, the iso-surface of Q equals 100 (Eq. 5) is calculated at the last time step of each case. The resulting vortex structures downstream of the net are shown in Fig. 6. The color represents the velocity variations. It is visible that the vortices are mainly distributed at the intersections, and the vortices around the net bars are less significant. Therefore, the resistance at each intersection might take a large proportion in the total resistance of net panels. In addition, the local acceleration of the flow at the center of each mesh and velocity reductions behind the knots are observed. Furthermore, it is meaningful to consider the interaction of the vortices, which is largely affect the hydrodynamics around the net panel. Due to the low solidity ratio and large hanging ratio of the mesh, the

interaction of surrounding vortices is not clear among the three-sized cases. Overall, considering the computational cost and accuracy, the 2×2 mesh pattern is used for further research on the impact of geometrical properties of the net meshes on the turbulence and hydrodynamics.

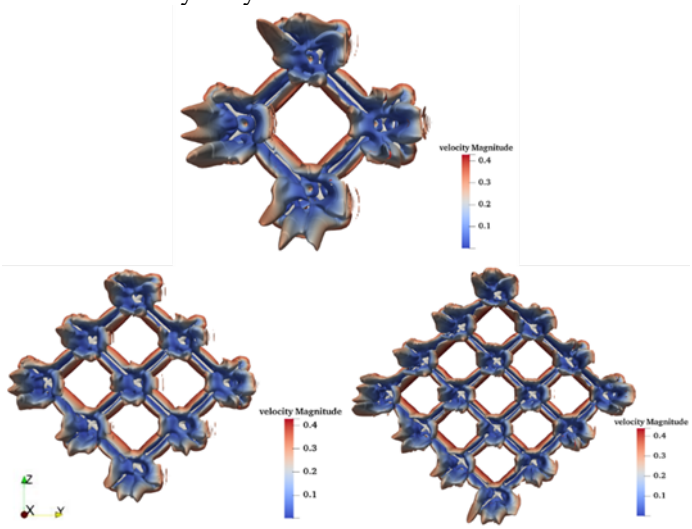

Figure 6: Iso-surface of Q=100 in three-sized meshes

3.2 Hydrodynamics and turbulence around net meshes with different Solidity ratio (S_n)

3.2.1 Hydrodynamics

The first way to change S_n is to change the diameter of the bars. Thus, Re is changed at the same time. In contrast, changing the length of the bars to control S_n, does not change Re. In order to found a relationship for C_d based on Re and S_n, more cases with a wider range of Re (800~2200) are carried out based on the second method to control S_n (Case 9~Case 31, shown in Table 2). Firstly, the relationship between C_d and Re are presented in Fig. 7a. Here, S_n is controlled by the length of the net bars. It can be seen that C_d shows an increasing trend with increasing S_n. Especially for S_n=0.2~0.3, the increasing rate is more than 20%. To a lesser extent, C_d increases firstly and then decreases gradually with Re when S_n is larger than 0.2. The dependences of Re and S_n on C_d in this research remain consistent with the results in [13] and [14]. Additionally, it is obvious that S_n has a more significant influence on C_d than Re. Based on these observations, polynomial regression is used to fit the simulation data. The resulting semi-empirical formula (Eq. 6) and the corresponding response surface (Fig. 7b) can be used to estimate C_d of nets with different S_n and Re. The fitting rate is 0.95, i.e., the goodness of fit is acceptable.

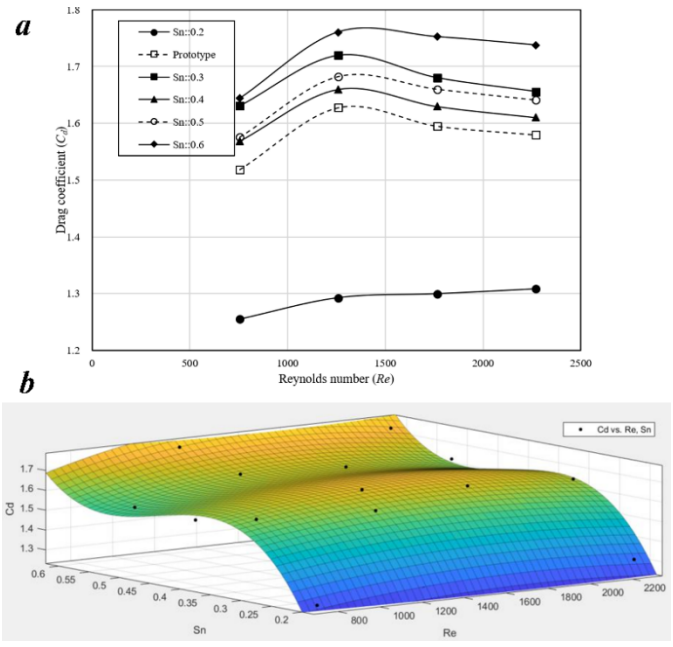

Figure 7: ***a.*** Relationship among C_d, Re and S_n (through length). ***b.*** Response surface between C_d, Re and S_n.

$$C_d = p00 + p10*Re + p01*S_n + p20*(Re\text{^}2) + p11*Re*S_n + p02*(S_n\text{^}2) + p21*(Re\text{^}2)*S_n + p12*Re*(S_n\text{^}2) + p03*(S_n\text{^}3) \quad (6)$$

Coefficients	Values
p00	-1.497
p10	0.0002193
p01	21.84
p20	-3.989e-08
p11	5.318e-05
p02	-52.25
p21	-1.697e-07
p12	0.0006487
p03	39.66

Moreover, the relevance about C_d, Re, and S_n on basis of changing diameter of twines was also studied (Fig. 8). C_d of some cases were much higher compared with the former results. It's not possible to use the same semi-empirical formulas fitted based on the previous method. Therefore, varied modes of changing S_n of net meshes had impacts on hydrodynamics to some degree.

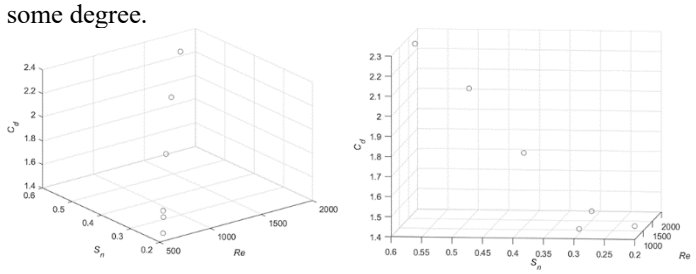

Figure 8: Relationship among C_d, Re and S_n (through diameter)

3.2.2 Turbulence around meshes with different Solidity ratio (S_n)

Two probe-lines in x direction, which is located in the regions of strong turbulence, were selected to study the velocity variations (see Fig. 9). Firstly, we set up S_n ranging from 0.2 to 0.6 by changing the diameter of net bar and keeping the length of all net bars consistent with the prototype. From Fig. 9, P1-the middle node of mesh shows that the velocity decreases fast without significant difference at the upstream area in all cases with various S_n, and reduces to 20% of the incoming velocity. Afterwards, it increases with different rates for varying S_n. The increasing rates for smaller S_n are 10% larger than that of cases with larger S_n, and the case with the smallest solidity ratio shows the largest downstream velocity. However, it is significant that larger S_n cases shows a greater increasing rate than that of smaller S_n cases around the mesh center. The flow in the largest S_n case is accelerated by more than 1.5 times the incoming velocity. It is explained by the larger radius of the cylinder resulting in an increased fluid separation and acceleration. After passing the meshes, the extent of velocity reduction of cases with larger S_n are more significant compared with that of smaller S_n cases. The interaction of the vortices at the downstream area for the large S_n cases yields a considerable velocity reduction which takes longer distance to achieve a steady state compared with small S_n cases. In the far-field, the velocity is in a steady state at value smaller than the incoming velocity except for the largest S_n case. The iso-surface of Q=100 in the cases of S_n equals 0.2, 0.4 and 0.6 are calculated and is shown in Fig. 10. No obvious interaction of vortices is observed in case of S_n=0.2, while interaction downstream increases with increasing S_n, which is in accordance with the explanations from above.

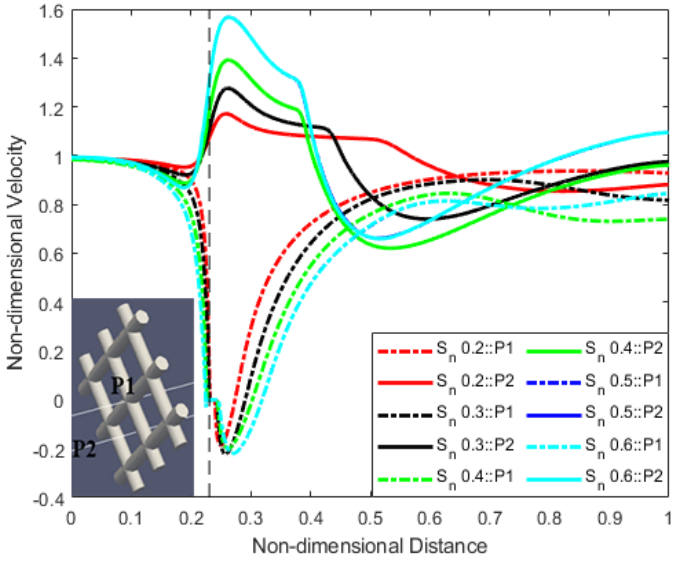

Figure 9: Non-dimensional velocity along the probe lines among cases with varied S_n (varied diameter)

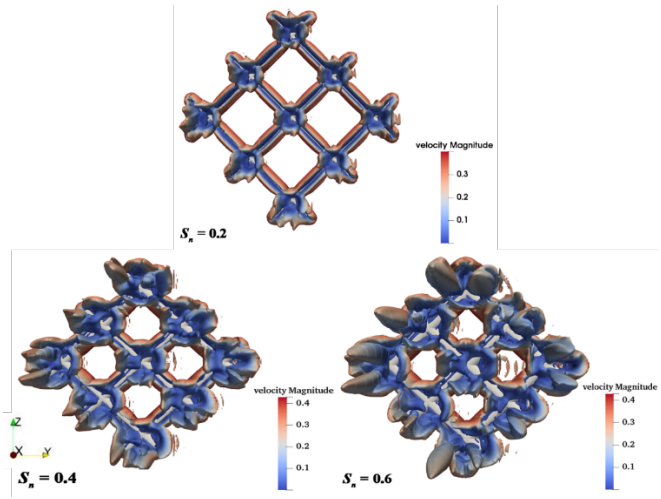

Figure 10: Iso-surface of Q=100 in the cases of which S_n = 0.2, 0.4 and 0.6

Next, the length of the net bars is changed to vary S_n between 0.2 and 0.6, while the diameter is kept constant. As presented in Fig. 11, the flow patterns are different from above, especially in the area after passing the mesh. P1 shows that the velocity decreases fast without significant change in the upstream area for all cases. Then, it increases gradually close to the values of the incoming velocity. For the larger S_n cases, the increasing processes at the downstream region shows fluctuations, which might be related to the greater vortex interaction in the wake region. Moreover, the velocities at the mesh center in all cases increase sharply at first and then decrease to the incoming velocity value. The maximum velocity due to local accelerations around the mesh in all S_n cases are the same, which is about 1.2~1.3 times the incoming velocity. After the flow passes the mesh, the velocity reduction is more obvious in larger S_n cases compared with smaller S_n cases. In the far-field, the velocity stabilizes to the value of the incoming velocity except for the case with S_n=0.3. The iso-surface of Q=100 for the cases with S_n equals 0.2, 0.4 and 0.6 are calculated and provided in Fig. 12. Again, no obvious interaction of the vortices in case of S_n=0.2 is given, while the interaction downstream can be observed with increasing S_n. Compared with the first method of changing S_n based on changing length of each twine, the interaction of the vortices is more significant for larger S_n. This accounts for the fact that the local acceleration around the mesh center (maximum 1.2~1.3 times of incoming velocity) based on changing the diameter of the bars is smaller than before (maximum 1.6 times of incoming velocity).

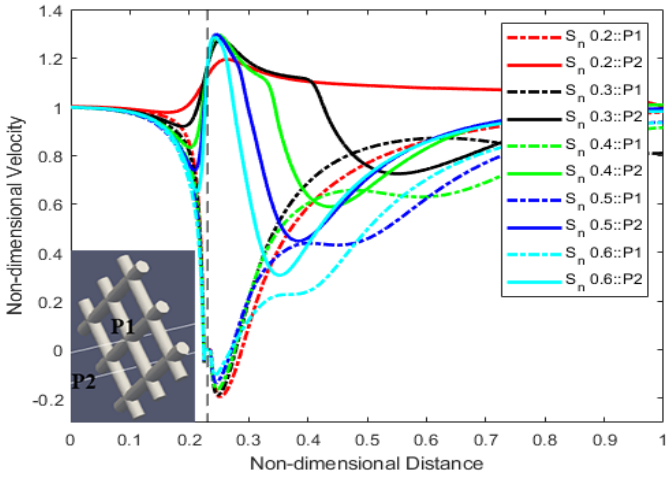

Figure 11: Non-dimensional velocity along the probe lines among cases with varied S_n (varied lengths)

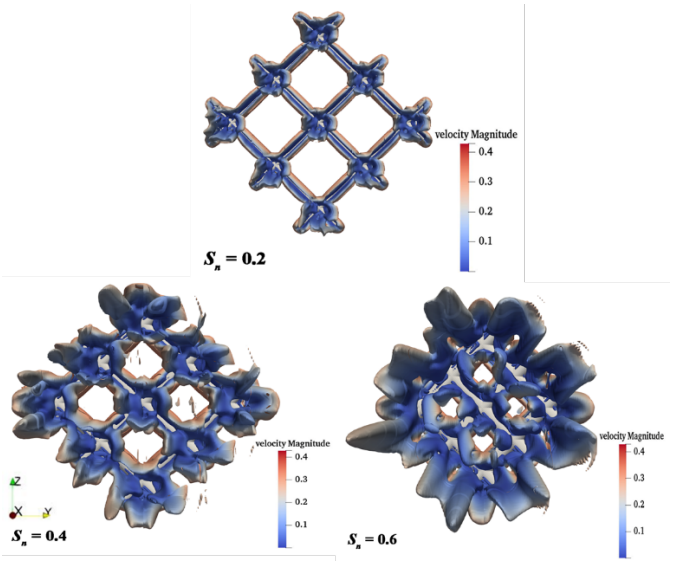

Figure 12: Iso-surface of Q=100 in the cases of which S_n = 0.2, 0.4 and 0.6

4 Conclusions and future work

In this paper, turbulence, hydrodynamics around net meshes and its related size, Solidity ratio (S_n) and Reynolds number (Re) were studied using REEF3D. Accuracy of results was validated through 2D cylinder cases and 3D cruciform cases. Conclusions were drawn as follows:

1) 2*2 or 3*3 mesh cases are more reliable when studying turbulence around net meshes, flow interactions around net bars, nodes or effects from other meshes should be taken into consideration.
2) Two patterns controlling S_n have different effects on flow around meshes.
3) Two patterns controlling S_n have different effects on the hydrodynamics of meshes. Semi-empirical formula about C_d, S_n, and Re was derived based on the mode, which is to change the length of the net bar to control S_n.

Other variables related to hydrodynamics, such as pressure coefficients, should also be analyzed in future studies. Furthermore, more factors concerning hydrodynamics and turbulence of meshes would be considered such as roughness of material, hanging ratio, angle of attack. It's recommended that the above structural parameters should be fitted to the semi-empirical formula, and provide a more comprehensive reference for the high-resolution numerical simulation of nets. In addition, more cases should be tested to derive the semi-empirical formula about C_d, S_n, and Re based on changing the diameter of the net bar to control S_n. In terms of turbulence model, dynamic sub-grid scale (SGS) LES model would be used to get more precise turbulence patterns or make the comparison with simulation results using URANS.

ACKNOWLEDGEMENTS

The study presented in the manuscript is supported by the National Key Research and Development Program of China (Project No. 2019YFD0901000). The authors are grateful for the State Foundation for Visiting Ph.D. student from China Scholarship Council (No. 201906330049). This research was supported in part with computational resources at NTNU provided by The Norwegian Metacenter for Computational Sciences (NOTUR, http://www.notur.no) under project no. NN2620K.

REFERENCES

[1] O.M., F., 2014, "Hydrodynamics of Marine and Offshore Structures," *J. Hydrodyn.*, (06), pp. 835–847.
[2] Zheng, Z. Q., Wan, R., Chang, Z. Y., Zhang, Y., and Tao, J., 2019, "Analysis of Plane Netting with Twine Breakage in Aquaculture Net Cage," *J. Mar. Sci. Technol.*, **27**(1), pp. 72–76.
[3] Li, L., Jiang, Z., Wang, J., and Ong, M. C., 2019, "Numerical Study on the Heading Misalignment and Current Velocity Reduction of a Vessel-Shaped Offshore Fish Farm," *J. Offshore Mech. Arct. Eng.*, **141**(5).
[4] CHOO Y, and CASARELLA MJ, 1971, "Hydrodynamic Resistance of Towed Cables," *J Hydronautics*, **5**(4), pp. 126–131.
[5] Miline P H, 1972, "Fish and Shelfish Farming in Coastal Waters," *Fishing News*, London, UK.
[6] Løland, G., 1993, "Current Forces on, and Water Flow through and around, Floating Fish Farms," *Aquac. Int.*, **1**(1), pp. 72–89.
[7] Zhan, J. M., Jia, X. P., Li, Y. S., Sun, M. G., Guo, G. X., and Hu, Y. Z., 2006, "Analytical and Experimental Investigation of Drag on Nets of Fish Cages," *Aquac. Eng.*, **35**(1), pp. 91–101.
[8] Zienkiewicz, O. C., 1980, "Viscous Flow."
[9] Balash, C., Colbourne, B., Bose, N., and Raman-Nair, W., 2009, "Aquaculture Net Drag Force and Added Mass," *Aquac. Eng.*, **41**(1), pp. 14–21.
[10] Hosseini, S. A., Lee, C. W., Kim, H. S., Lee, J., and Lee, G. H., 2011, "The Sinking Performance of the Tuna Purse Seine Gear with Large-Meshed Panels Using Numerical Method," *Fish. Sci.*, **77**(4), pp. 503–520.

[11] Kristiansen, T., and Faltinsen, O. M., 2012, "Modelling of Current Loads on Aquaculture Net Cages," *J. Fluids Struct.*, **34**, pp. 218–235.
[12] Lader, P., Enerhaug, B., Fredheim, A., Klebert, P., and Pettersen, B., 2014, "Forces on a Cruciform/Sphere Structure in Uniform Current," *Ocean Eng.*, **82**, pp. 180–190.
[13] Zhou, C., Xu, L., Hu, F., and Qu, X., 2015, "Hydrodynamic Characteristics of Knotless Nylon Netting Normal to Free Stream and Effect of Inclination," *Ocean Eng.*, **110**, pp. 89–97.
[14] Tang, H., Hu, F., Xu, L., Dong, S., Zhou, C., and Wang, X., 2017, "The Effect of Netting Solidity Ratio and Inclined Angle on the Hydrodynamic Characteristics of Knotless Polyethylene Netting," *J. Ocean Univ. China*, **16**(5), pp. 814–822.
[15] Patursson, Ø., Swift, M. R., Tsukrov, I., Baldwin, K., and Simonsen, K., 2006, "Modeling Flow through and around a Net Panel Using Computational Fluid Dynamics," *Ocean.* 2006, (2), pp. 2–6.
[16] Zhao, Y. P., Bi, C. W., Dong, G. H., Gui, F. K., Cui, Y., Guan, C. T., and Xu, T. J., 2013, "Numerical Simulation of the Flow around Fishing Plane Nets Using the Porous Media Model," *Ocean Eng.*, **62**, pp. 25–37.
[17] Bi, C. W., Zhao, Y. P., Dong, G. H., Xu, T. J., and Gui, F. K., 2014, "Numerical Simulation of the Interaction between Flow and Flexible Nets," *J. Fluids Struct.,***45**, pp. 180-201.
[18] Chen, H., and Christensen, E. D., 2017, "Development of a Numerical Model for Fluid-Structure Interaction Analysis of Flow through and around an Aquaculture Net Cage," *Ocean Eng.*, **142**, pp. 597–615.
[19] Bi, C. W., Balash, C., Matsubara, S., Zhao, Y. P., and Dong, G. H., 2017, "Effects of Cylindrical Cruciform Patterns on Fluid Flow and Drag as Determined by CFD Models," *Ocean Eng.*, **135**(March 2016), pp. 28–38.
[20] Bihs, H., Kamath, A., Alagan Chella, M., Aggarwal, A., and Arntsen, Ø. A., 2016, "A New Level Set Numerical Wave Tank with Improved Density Interpolation for Complex Wave Hydrodynamics," *Comput. Fluids*, **140**, pp. 191–208.
[21] Kamath, A., Chella, M. A., Bihs, H., and Arntsen, O. A., 2015, "Evaluating Wave Forces on Groups of Three and Nine Cylinders Using a 3D Numerical Wave Tank," *Eng. Appl. Comput. Fluid Mech.*, **9**(1), pp. 343–354.
[22] Martin, T., Kamath, A., and Bihs, H., 2020, "Modeling and Simulation of Moored-Floating Structures Using the Tension Element Method," *J. Offshore Mech. Arct. Eng.*, **142**(1).
[23] Wilcox, D. C., 1993, Turbulence Modeling for CFD.
[24] Fu, W. S., Lai, Y. C., and Li, C. G., 2013, "Estimation of Turbulent Natural Convection in Horizontal Parallel Plates by the Q Criterion," *Int. Commun. Heat Mass Transf.*, **45**, pp. 41–46.
[25] Hunt, J. C. R., Wray, a a, and Moin, P., 1988, "Eddies, Streams, and Convergence Zones in Turbulent Flows," *Cent. Turbul. Res. Proc. Summer Progr.*, (1970), pp. 193–208.
[26] Stringer, R. M., Zang, J., and Hillis, A. J., 2014, "Unsteady RANS Computations of Flow around a Circular Cylinder for a Wide Range of Reynolds Numbers," *Ocean Eng.*, **87**, pp. 1–9.
[27] Faltinsen, O. M., 2017, "Sloshing," Adv. Mech., **47**(1), pp. 1–24.
[28] Zdravkovich, M. M., 1990, "Conceptual Overview of Laminar and Turbulent Flows Past Smooth and Rough Circular Cylinders," *J. Wind Eng. Ind. Aerodyn.*, **33**(1–2), pp. 53–62.
[29] MASSEY, B. S., 1975, "MECHANICS OF FLUIDS," ((3RD ED. 1975)).
[30] Anon, 1981, "MEAN FORCES, PRESSURES AND FLOW FIELD VELOCITIES FOR CIRCULAR CYLINDRICAL STRUCTURES: SINGLE CYLINDER WITH TWO-DIMENSIONAL FLOW.," *Eng. Sci. Data Unit*, Data Items.
[31] Norberg, C., 2003, "Fluctuating Lift on a Circular Cylinder: Review and New Measurements," *J. Fluids Struct.*, **17**(1), pp. 57–96.
[32] Achenbach, E., and Heinecke, E., 1981, "On Vortex Shedding from Smooth and Rough Cylinders in the Range of Reynolds Numbers 6×103 to 5×106," *J. Fluid Mech.*, **109**(12), pp. 239–251.
[33] Aggarwal, A., Bihs, H., Myrhaug, D., and Chella, M. A., 2019, "Characteristics of Breaking Irregular Wave Forces on a Monopile," *Appl. Ocean Res.*, 90.
[34] Alagan Chella, M., Bihs, H., and Myrhaug, D., 2019, "Wave Impact Pressure and Kinematics Due to Breaking Wave Impingement on a Monopile," *J. Fluids Struct.*, **86**, pp. 94–123.
[35] Aggarwal, A., Bihs, H., Shirinov, S., and Myrhaug, D., 2019, "Estimation of Breaking Wave Properties and Their Interaction with a Jacket Structure," *J. Fluids Struct.*, 91.
[36] Martin, T., Kamath, A., and Bihs, H., 2019. Numerical Modelling of the Interaction between a Fish Net and Fluid using CFD. *Proceedings of VII International Conference on Computational Methods in Marine Engineering, MARINE 2019*, Gothenburg, Sweden.
[37] Martin, T., Kamath, A., and Bihs, H., 2019. Numerical Modelling of Net Motion in Waves and Current Using CFD. *Proceedings of 38th International Conference on Ocean, Offshore and Arctic Engineering, OMAE 2019.Volume 6. Glasgow, UK.*
[38] Fredheim, A., 2005. Current Force on Net Panels. *Doctoral Thesis*, Norwegian University of Science and Technology, Trondheim.